ADVANCED MATERIALS
www.advmat.de

Multifunctional Organic-Semiconductor Interfacial Layers for Solution-Processed Oxide-Semiconductor Thin-Film Transistor

Guhyun Kwon, Keetae Kim, Byung Doo Choi, Jeongkyun Roh, Changhee Lee, Yong-Young Noh, SungYong Seo, Myung-Gil Kim, and Choongik Kim**

The stabilization and control of the electrical properties in solution-processed amorphous-oxide semiconductors (AOSs) is crucial for the realization of cost-effective, high-performance, large-area electronics. In particular, impurity diffusion, electrical instability, and the lack of a general substitutional doping strategy for the active layer hinder the industrial implementation of copper electrodes and the fine tuning of the electrical parameters of AOS-based thin-film transistors (TFTs). In this study, the authors employ a multifunctional organic-semiconductor (OSC) interlayer as a solution-processed thin-film passivation layer and a charge-transfer dopant. As an electrically active impurity blocking layer, the OSC interlayer enhances the electrical stability of AOS TFTs by suppressing the adsorption of environmental gas species and copper-ion diffusion. Moreover, charge transfer between the organic interlayer and the AOS allows the fine tuning of the electrical properties and the passivation of the electrical defects in the AOS TFTs. The development of a multifunctional solution-processed organic interlayer enables the production of low-cost, high-performance oxide semiconductor-based circuits.

Increasing demands for next-generation, large-area electronics have motivated significant research efforts toward the development of new semiconductors and innovative processing techniques for thin-film transistors (TFTs) with high electrical performance, multifunctionalities, and a low fabrication cost.[1] High-performance, low-cost multifunctional TFTs have been successfully demonstrated with newly emerging semiconductors (organic semiconductors (OSCs), carbon materials (carbon nanotubes, graphene, C_{60}), oxide semiconductors, etc.) and low-cost solution-processing methods (spin-coating, ink-jet printing, spray-coating, etc.) for flexible electronics, transparent electronics, and optoelectronics applications.[2] Among the various semiconductors, sputter-deposited amorphous indium–gallium–zinc oxide (a-IGZO) TFTs have been successfully implemented as the backplane component of fast-switching high-resolution displays and high current-driven organic light-emitting diode displays because of their high electrical performance (electron mobility (μ_e) > 10 cm^2 V^{-1} s^{-1} and current on/off ratio (I_{on}/I_{off}) > 10^6) and good electrical uniformity due to their homogenous amorphous structure.[3] Furthermore, solution-processed a-IGZO TFTs have high electrical performance with a mobility over 10 cm^2 V^{-1} s^{-1} and an I_{on}/I_{off} over 10^6 with a processing temperature as low as 150 °C, which are comparable to the values for vacuum-processed oxide-semiconductor TFTs and superior to those of conventional a-Si-based TFTs.[4]

In spite of the superior intrinsic electrical performance of a-IGZO TFTs, the efficient passivation of the channel layer from extrinsic impurities and the facile electrical-property control of these devices must be overcome for further applications in low-cost, large-area electronics, such as displays, sensor arrays, and printed logic circuits. For instance, copper-ion diffusion in TFTs with copper electrodes is a critical issue for the reduction of the RC delay, which is crucial for the realization of TFT circuits with a high switching speed.[5] Copper ions migrate into the oxide-semiconductor channel layer because of electrical or thermal stresses, which results in the significant electrical performance degradation of metal-oxide semiconductor TFTs with copper electrodes. Tailing and deep trap states formed by copper ions

G. Kwon, K. Kim, Prof. C. Kim
Department of Chemical and Biomolecular Engineering
Sogang University
35 Baekbeom-ro, Mapo-gu, Seoul 04107, Republic of Korea
E-mail: choongik@sogang.ac.kr

B. D. Choi, Prof. M.-G. Kim
Department of Chemistry
Chung-Ang University
84 Heukseok-ro, Dongjak-Gu, Seoul 06974, Republic of Korea
E-mail: myunggil@cau.ac.kr

DOI: 10.1002/adma.201607055

J. Roh, Prof. C. H. Lee
Department of Electrical and Computer Engineering
Inter-University Semiconductor Research Center (ISRC)
Seoul National University
1 Gwanak-ro, Gwanak-gu, Seoul 08826, Republic of Korea

Prof. Y.-Y. Noh
Department of Energy and Materials Engineering
Dongguk University
30 Pildong-ro 1-gil, Jung-gu, Seoul 04620, Republic of Korea

Prof. S.Y. Seo
Department of Chemistry
Pukyong National University
45 Yongso-ro, Namgu Pusan 48513, Republic of Korea

in metal-oxide semiconductors cause hump-like behavior in the transfer characteristics, as well as electrical instabilities of TFTs.[6] Refractory metal-based barrier layers have been deposited between the copper electrode and metal oxide via expensive sputtering deposition.[7] Novel barrier layers preventing copper diffusion fabricated by low-cost solution deposition should be developed for next-generation large-area electronics.

The doping-level control of oxide semiconductors is crucial for achieving the proper turn-on voltage and Ohmic-contact formation in TFT devices. However, the electronic properties of amorphous-oxide semiconductors (AOSs) are poorly controlled by conventional doping methods because the lack of structural ordering in AOSs prohibits the implementation of typical substitutional doping.[8] Alternatively, shallow donor states arising from oxygen vacancies in AOSs generally allow the control of the free-electron concentration, but the inevitable generation of deep trap states from the vacancies induce electrical-performance degradation in TFTs, such as a low electron mobility and bias instability.[9] Moreover, the adsorption of ambient molecules (H_2O, O_2, etc.) on the oxygen vacancies in AOSs induces defect states, degrading the electrical performance and stability of AOS-based TFTs. Various passivation layers, such as dielectric oxides (SiO_2 and Al_2O_3), SiN_x, and composite materials, have been investigated for the stabilization of a-IGZO TFTs against environmental effects.[10] Unfortunately, the aforementioned inorganic passivation layers typically based on plasma-enhanced chemical vapor deposition may degrade the electrical properties of AOSs because of the plasma-induced radiation damage to the channel region. Therefore, investigation of an effective passivation layer—formed by a soft processing method—that can control the electrical properties of oxide TFTs without composition tuning is essential for achieving reliable AOS-based TFTs.

In this regard, we report OSC interfacial layers (IFLs) with multifunctionality for AOS-based TFTs. By employing OSC IFLs prepared via a simple solution process, we successfully prevented copper-ion migration into the AOS, controlled the electrical properties of the AOS, and passivated the AOS from environmental effects and electrical stress. Furthermore, the contact resistance caused by OSC IFLs was reduced by the molecular doping of the OSCs.

Figure 1a shows a schematic of the effective channel passivation of a-IGZO with OSC IFLs. Because the metal electrodes with a low resistivity, which form Ohmic contacts with the a-IGZO semiconductor, are essential for a high-performance TFT circuit, various metals (Al, Cu, Ag, Au, and Mo)[11] and conducting oxides (a-IZO, ITO, In_2O_3)[12] have been investigated as potential electrodes for a-IGZO TFTs. In particular, copper is considered as the most suitable candidate for the electrodes, considering that its resistivity (1.7 μΩ cm) is comparable to that of silver (1.6 μΩ cm), while it is 100 times cheaper than silver.[13] To prevent the significant electrical-performance degradation of AOS-based TFTs with copper electrodes, the copper ion-blocking layer should physically or chemically hinder the ion migration. Refractory metals with high melting points, such as Mn, W, Ta, and Mo,[7] have been employed as a barrier layer between the copper electrode and the metal-oxide semiconductor. For instance, zinc-tin-oxide (ZTO) TFTs with a tantalum barrier film for copper source/drain (S/D) electrodes showed an improved subthreshold swing (SS) and electron mobility.[14] Unfortunately, the rigid physical barrier due to refractory-metal IFLs inherently requires expensive sputtering deposition and is incompatible with low-cost solution-processing methods. In general, π-electron rich species can be considered as soft bases, which can interact strongly with soft-acid species, such as low-valent transition-metal cations and heavy-metal cations.[15]

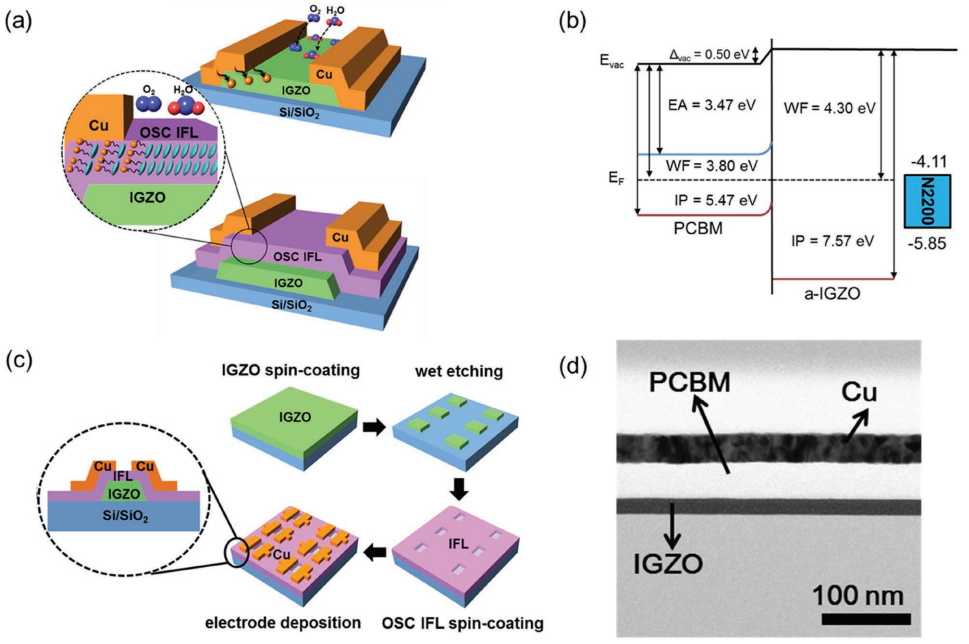

Figure 1. a) Schematics showing the device structures of a-IGZO TFTs with and without OSC IFLs. b) Schematic of the band alignment of a-IGZO and OSC IFLs (PCBM and N2200). c) Schematic of the device-fabrication process for a-IGZO TFTs via a solution process. d) Cross-sectional transmission electron microscopy (TEM) image of an a-IGZO TFT with a PCBM IFL.

Unlike the case of typical copper ion-blocking layers made of physically dense refractory metals, strong chemical binding between Cu^+ and π-electron-rich OSC can effectively prevent the penetration of copper ions into the channel layer of AOSs.

As shown in Figure 1a, the adsorption of ambient chemical species is the critical issue for the realization of electrically stable high-performance solution-processed AOS-based TFTs. Environmental species such as oxygen and water are easily adsorbed on the oxygen-vacancy sites in the oxide semiconductors.[16] During the oxygen-molecule adsorption on oxide semiconductors, electrons in the conduction band of the semiconductor are transferred to oxygen, forming O_2^- or O^-. Consequently, a depletion layer is formed under the oxide surface, shifting the threshold voltage (V_{th}) in TFTs.[17] In contrast to oxygen molecules, water molecules act as donors in oxide semiconductors, changing the electrical properties of TFTs.[18] As an environmental species-blocking layer, the soft OSC can fill the empty coordination sites of the metal cation (i.e., oxygen vacancies) in AOSs via strong interactions with the soft metal (indium), suppressing the facile adsorption of water and oxygen on the vacancy sites of AOSs.[16] Moreover, the hydrophobic nature of OSCs can hinder the adsorption of water on the AOSs. Overall, thin OSC IFLs are efficient for blocking copper migration as well as contamination by external ambient species that significantly degrade the electrical performance and stability of oxide semiconductor-based TFTs.

In addition to the passivation of oxide semiconductors, OSC IFLs can be applied to control the electrical properties of AOSs. Recent reports on the charge-transfer doping and the band alignment between a crystalline oxide semiconductor and organic materials provide avenues for controlling the electrical properties of AOSs without electrical-performance degradation.[19,20] The charge transfer at the organic–inorganic heterojunction has been extensively investigated to achieve efficient charge collection or insertion with OSCs.[20,21] Figure 1b and Figure S1 (Supporting Information) show the electronic structure of a-IGZO and OSC IFLs including small molecules (phenyl-C61-butyric acid methyl ester: PCBM) and a polymer (poly{[*N*,*N*′-bis(2-octyldodecyl)-naphthalene-1,4,5,8-bis(dicarboximide)-2,6-diyl]-alt-5,5′-(2,2′-bithiophene)}: N2200). Considering the universality of charge-transfer phenomena between inorganic and OSCs, diverse OSCs can be applied to tune the electrical properties of oxide semiconductors and even AOSs.

As shown in Figure 1c, the integration of OSC IFLs between an oxide semiconductor and metal electrodes was achieved via the simple solution processing of metal-oxide and OSC layers. A soluble metal-oxide precursor for a-IGZO was spin-coated onto n^{++}-Si/300 nm SiO_2 substrates and then annealed at 320 °C. In general, electrical characteristics of oxide semiconductor TFT devices can be improved by introducing thin and high-k dielectrics, such as Al_2O_3, ZrO_2, and HfO_2.[22] In our study, however, we focused on the improving the stability of solution processed TFT devices and therefore 300 nm SiO_2 was used as the dielectric which is suitable for high voltage stress tests. Subsequently, a soluble OSC layer was spin-coated and annealed at 50–120 °C. The complete solution processability of electrical components is critical for the realization of low-cost printed electronics.[23] The smooth surface and amorphous nature of the solution-processed a-IGZO layer were confirmed by atomic force microscopy in Figure S2a (Supporting Information) and grazing-incidence X-ray diffraction (GIXRD) in Figure S3a (Supporting Information), respectively. The cross-sectional TEM image shown in Figure 1d demonstrates the sharp interface between the OSC IFLs and AOSs.

The OSC IFLs effectively protected the metal-oxide semiconductor from copper-ion migration and contamination by environmental species. **Figure 2**a,b shows the typical transfer-curve evolution of a-IGZO TFTs with and without OSC IFLs upon

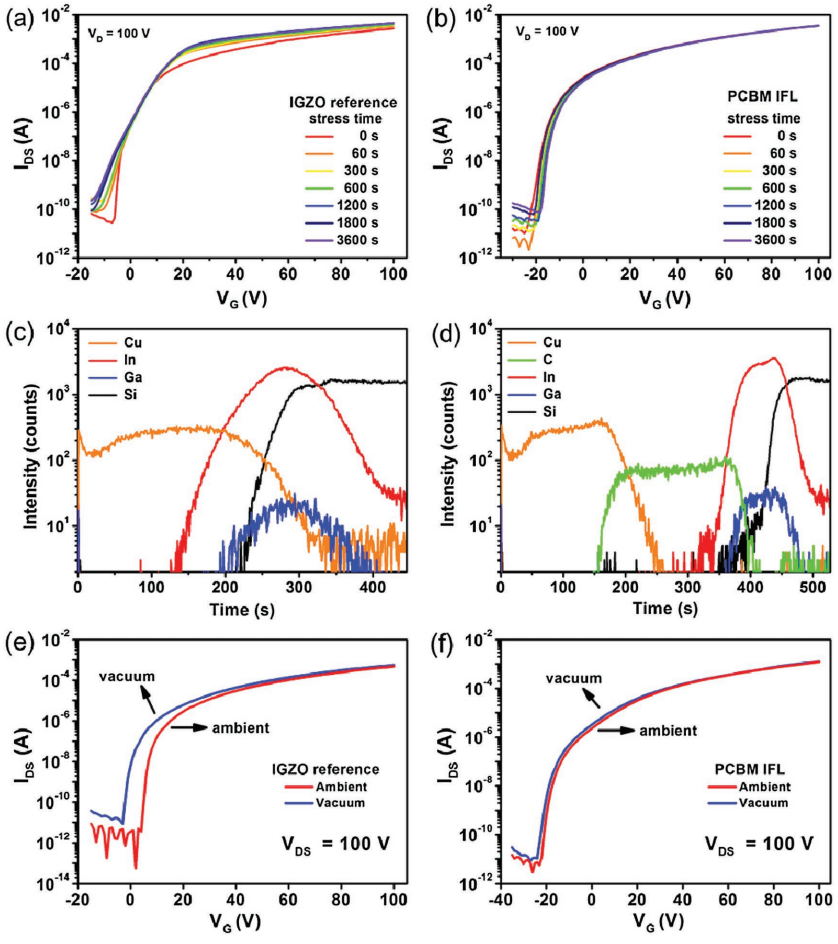

Figure 2. Variations of the I_{DS}–V_G transfer characteristics for a) a-IGZO reference TFTs and b) a-IGZO TFTs with PCBM IFL with respect to the stress time under a drain bias of 100 V. Time-of-flight (TOF) secondary ion mass spectrometry (SIMS) depth profiles of c) Cu/a-IGZO/Si, and d) Cu/PCBM/a-IGZO/Si multilayers. The I_{DS}–V_G transfer characteristics for e) a-IGZO reference TFTs and f) a-IGZO TFTs with PCBM IFLs under ambient and vacuum conditions.

the application of continuous electrical stress on copper S/D electrodes for 1 h. Initially, the reference a-IGZO TFTs without OSC IFLs exhibited an electron mobility of 2.72 $cm^2 V^{-1} s^{-1}$, an I_{on}/I_{off} of 10^8, a V_{th} of 1.95 V, and an SS of 1.01 V dec^{-1} (Table S1, Supporting Information). With an applied electrical field, copper ions penetrated into the metal-oxide channel layer, which is common for silicon-based microelectronic devices and oxide semiconductor-based macroelectronic devices employing copper electrodes.[24] As previously reported, the migrating copper ions in a-IGZO can generate either acceptor- or donor-like trap states.[6] The large SS and V_{th} shift of 4.08 V dec^{-1} and −18.98 V, respectively, after 1 h of electrical stress reveal the generation of deep trap and donor states by copper-ion diffusion (Table S2, Supporting Information). In contrast, the transfer characteristics of the a-IGZO TFTs with PCBM IFLs afforded an electrically stable TFT device (Figure 2b and Table S2, Supporting Information). Unlike the large negative V_{th} shift induced by copper-ion migration in the reference device, the small positive V_{th} shift for the devices with OSC IFLs reveals that the copper-ion migration is negligible in a-IGZO with OSC IFLs (Table S2, Supporting Information). The stability of OSC IFL-based TFTs is also confirmed by the field-dependent transfer characteristics (Figure S4, Supporting Information). As shown, copper-ion migration was observed for a-IGZO TFTs without OSC IFLs as V_{DS} was increased from 1 to 100 V. For a-IGZO reference TFTs (with channel length of 25 μm), copper-ion migration is clearly observed as humplike behavior at $V_{DS} > 90$ V (3.6 MV m^{-1}) (Figure S4a, Supporting Information), as reported in the literature.[6] On the other hand, a-IGZO TFTs with OSC IFLs exhibited stable device operation without any humplike behavior (Figure S4b,c, Supporting Information). The OSC IFLs sufficiently blocked the copper-ion movement via the chemical interaction between the copper ions and the OSC. According to the hard soft acid base (HSAB) theory, Cu^+ can be considered as a soft acid, which can strongly interact with a soft base, such as lone pairs of electrons on S and P atoms and delocalized π-electrons in the OSCs.[15] Similar electrical stability was observed for a-IGZO devices with other OSC IFLs, such as the n-type polymer N2200 (Figures S4c and S5a, Supporting Information). The SIMS spectra of Cu/PCBM/a-IGZO/Si and Cu/a-IGZO/Si multilayer structures indicate that copper-ion penetration was effectively suppressed (Figure 2c,d). To facilitate copper-ion penetration into the oxide-semiconductor layer, the multilayer structures were heated at 150 °C for 60 min. The SIMS signal of the a-IGZO reference device shown in Figure 2c indicates that the copper signal was consistently detected with indium and gallium signals. Without the OSC IFLs, the copper ions penetrated into the whole a-IGZO layer, down to the oxide–silicon interface. On the other hand, copper ions could not penetrate into the a-IGZO layer when the PCBM layer was inserted as a blocking layer (Figure 2d). Overall, the OSC IFLs effectively blocked the copper-ion diffusion, not only under electrical stress but also under harsh heating conditions.

The efficient barrier property of the OSC IFLs against ambient species, such as water and oxygen, was also confirmed (Figure 2e,f). Transfer curves of the a-IGZO reference device show a large negative shift of the curves with the environmental change from ambient to vacuum (Figure 2e), which is mainly attributed to the desorption of water and oxygen from the semiconductor. The thin PCBM layer effectively blocked the adsorption of water and oxygen on the a-IGZO. In contrast to the large V_{th} shift of −7.21 V for the a-IGZO reference device (Figure 2e), the device with PCBM IFLs exhibited a negligible transfer-curve shift with a V_{th} shift of −0.43 V (Figure 2f). Regardless of the environment in which the measurements were performed, similar stable transfer curves of devices with N2200 IFLs were measured, as shown in Figure S5b (Supporting Information). In addition, the implementation of PCBM IFL into a-ZTO TFT devices showed the stable electrical performance under air and vacuum (Figure S6, Supporting Information), which confirmed that the OSC IFL could be generally applicable for various oxide semiconductors.

As shown in **Figure 3**a, and Figure S7 and Tables S1 and S4 in the Supporting Information, the multifunctionality of the OSC interlayer was utilized to tune the electrical characteristic of the AOSs. Figure S7 and Table S1 (Supporting Information) show that the V_{on} values shifted to negative values as the work function of the OSC decreased. Because PCBM and N2200, as well-known n-type OSCs with low lowest-unoccupied-molecular-orbital levels, allowed electron transfer from OSCs to a-IGZO, the ΔV_{on} values of the a-IGZO TFT devices were −20 and −15 V for PCBM and N2200, respectively. As shown in Figure 1b, the PCBM has a smaller work function than the N2200, which facilitates electron transfer into the IGZO layer, resulting in larger ΔV_{on} values. On the other hand, as shown in Figures S1 and S8 in the Supporting Information, electrical characteristics of the a-IGZO TFT are quite consistent regardless of the thickness of PCBM IFL above critical thickness (≈10 nm). However, because the IFL needs to act as a barrier to the atmospheric environment, the IFLs for all the TFT stability tests were deposited to a thickness of 34 nm. Considering the diverse electronic structures of OSCs, the electrical properties of AOSs should be tailored to targeted values using finely tuned organic materials. For instance, proper energy level of OSCs would ensure the passivation of electrical defect state within AOSs, while avoiding conducting oxide channel layer at the same time. Furthermore, high electron mobility of AOSs would be favorable for the efficient injection of electrons into channel layer in AOSs. Moreover, as observed in crystalline ZnO,[20] the n-doping of OSC IFLs can be utilized to tune the electrical properties of a-IGZO. As shown in Figure 3a, the controlled doping of PCBM with 4-(1,3-dimethyl-2,3-dihydro-1H-benzoimidazol-2-yl)phenyl)dimethylamine (N-DMBI)—a solution-processable n-type dopant—could change the degree of doping in a-IGZO, regardless of its crystallinity. Notably, the important aspect of the n-doping of PCBM was observed with the significant reduction of the contact resistance between a-IGZO and PCBM (Figure 3b and Figure S9, Supporting Information). The output curves of a-IGZO TFTs with undoped OSC interlayer shown in Figure S9 in the Supporting Information exhibit a more suppressed shape in the low-voltage region than the reference devices, which suggests a large contact resistance with the OSC IFL. By doping PCBM with N-DMBI, the contact resistance of the resulting device extracted by the well-known transmission line method (TLM)[25] was decreased from 4.62 kΩ cm (without N-DMBI) to 0.43 kΩ cm (doped with 2% N-DMBI) because of the strongly n-doped interface between the PCBM and a-IGZO and the reduced bulk resistance of the PCBM and

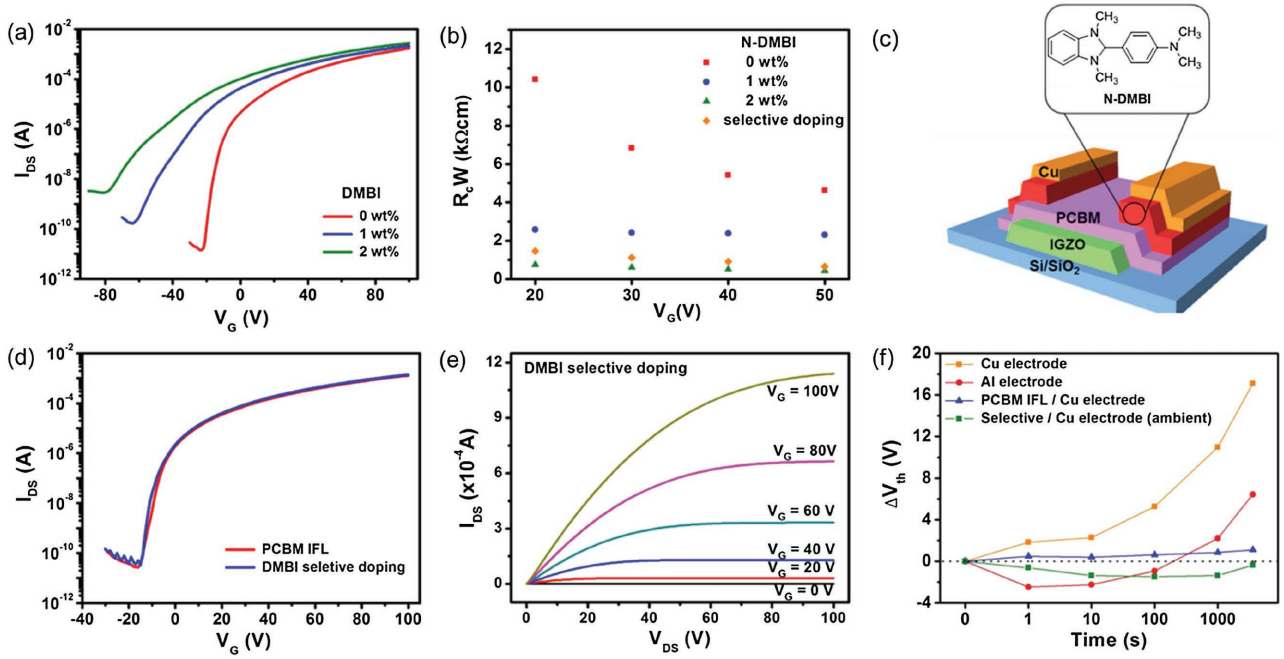

Figure 3. a) I_{DS}–V_G transfer characteristics of a-IGZO TFTs with N-DMBI-doped PCBM IFL at various doping concentrations. b) Gate-voltage dependence of the contact resistance for a-IGZO TFTs with PCBM IFLs at different doping concentrations and selectively doped with N-DMBI. c) Schematics showing the device structures of a-IGZO TFTs selectively doped with N-DMBI on S/D contact areas. d,e) I_{DS}–V_G and output characteristics of a-IGZO TFTs selectively doped with N-DMBI. f) V_{th} variation of various TFTs (a-IGZO TFTs with copper electrodes, aluminum electrodes, PCMB IFLs + copper electrodes, and selectively doped PCBM IFLs + copper electrodes) with respect to time under a positive gate bias stress (V_{DS} = 25 V, V_G = 50 V).

a-IGZO (Figure 3b, and Figures S10 and S11, Supporting Information)).[26] Although the n-doped PCBM multifunctional layer provided an excellent low-contact resistance interface and good passivation, the significant negative V_{th} shift is not desirable for typical TFT operation. To simultaneously achieve a low contact resistance and proper V_{th} values for a-IGZO TFTs, we fabricated spatially selectively doped PCBM IFLs/a-IGZO devices with a thermally evaporated N-DMBI dopant, as shown in Figure 3c. The thickness of the deposited N-DMBI was 2 nm, which corresponds to about 6 wt% doping for PCBM of 34 nm thickness when treated with thermal diffusion process. Doping concentration was enough to induce metallic contact, as reported in previous studies.[26] As shown in Figure 3d,e, and Figure S11d in the Supporting Information, the selective doping of PCBM with N-DMBI in the S/D contact area did not shift the V_{th} values compared with intrinsic PCBM, whereas the contact resistance was significantly reduced to 0.65 kΩ cm.

In addition to a high electron mobility and environmental stability, the intrinsic electrical stability of a-IGZO TFTs under electrical stress is crucial for the industrial implementation of solution-processed devices. Under the positive-bias-stress (PBS) condition, the oxygen adsorption on the back channel generates acceptor-like electron trap states.[27] These states can be removed by applying an electron-donating passivation layer at the oxygen-binding sites. As previously mentioned, PCBM can function as a passivation layer for device stabilization without generating additional defects from harsh vacuum processing conditions. As shown in Figure 3f and Figure S12 in the Supporting Information, a-IGZO TFTs with copper electrodes kept under the PBS condition (V_{DS} = 25 V, V_G = 50 V) for 3600 s exhibited a more significant transfer-curve shift of ΔV_{th} = 17.1 V than a-IGZO TFTs with aluminum-electrode devices (ΔV_{th} = 6.44 V). The larger V_{th} shift of the a-IGZO TFTs with copper electrodes, even under vacuum, is attributed to the intrinsic acceptor-like midgap states and the additional acceptor states due to copper-ion migration. As expected, the OSC IFLs significantly enhanced the electrical bias stability of the a-IGZO TFT with copper electrodes under the PBS condition. After 3600 s under the same PBS condition, the a-IGZO TFT with a PCBM IFL exhibited a very small ΔV_{th} of 1.11 V, which is comparable to that of vacuum-deposited a-IGZO.[28] Similar to our results, the effect of an electron-donating defect-passivation layer was demonstrated with Y_2O_3, which is regarded as a basic metal oxide.[29] Overall, the exceptional multifunctionality of OSC IFLs allows electrically and environmentally stable a-IGZO devices. After a PBS test under ambient conditions for 3600 s, the selectively doped PCBM IFL device exhibited a negligible ΔV_{th} of 0.36 V, as shown in Figure 3f. The long term stability of these PCBM IFL devices to the ambient environment is consistent with previous reports[26] in which DMBI also contributes to enhancing the air stability of PCBM. Considering the exceptional device stability of the a-IGZO with an inserted OSC IFL against chemical-species penetration and electrical stress, the solution-processed hybrid device with an OSC and AOS synergistically improves the electrical and environmental stabilities of solution-processed TFTs, which can enable the fabrication of low-cost and high-performance next-generation electronics.

We demonstrated that OSC-based IFLs are a multifunctional material suitable for the tuning and optimization of high-performance AOS-based TFTs. Considering the diversity

of OSCs and universality of charge-transfer phenomena, the OSC IFL-based organic-oxide hybrid structure is generally applicable for the fine tuning of the electrical properties of AOSs, such as the turn-on voltage and contact resistance. Using PCBM and N2200, we tuned the V_{on} from −4 to −24 V. Furthermore, a significant contact-resistance reduction from 4.62 to 0.43 kΩ cm was achieved with N-DMBI-doped PCBM. The OSC IFLs are excellent thin-film passivation layers for environmental species, ion diffusion, and electrical stress. The a-IGZO passivated with the OSC IFL had excellent stability regardless of the measurement conditions, such as ambient and vacuum conditions. The electrical stability of OSC IFL-passivated devices was improved from $\Delta V_{th} = -18.98$ to 1.36 V with a copper electrode, which is attributed to the blocking of the copper-ion diffusion and the midgap state passivation. The synergetic combination of the intrinsic chemical properties of the copper electrode, AOS, and OSC yielded electrically stable and high-performance hybrid devices. In summary, the solution-processed OSC interlayer provided a soft-passivation method for the high-performance copper electrode-based a-IGZO.

Experimental Section

Material Preparation and Device Fabrication: A 0.2 M mixture of indium nitrate hydrate ($In(NO_3)_3{\cdot}xH_2O$, 99.999%), gallium nitrate hydrate ($Ga(NO_3)_3{\cdot}xH_2O$, 99.999%), and zinc nitrate hydrate ($Zn(NO_3)_2{\cdot}xH_2O$, 99.999%), dissolved in 2-methoxyethanol (HPLC grade), was used as a precursor. The total mole ratio of In, Ga, and Zn was 60:20:20. All regents for the a-IGZO precursor solution were purchased for Sigma-Aldrich. The precursor solutions were stirred at 70 °C for 1 h and at room temperature for 3 h before use. To fabricate the device, highly N-doped silicon wafers (n^{++}-Si) were used as gate electrodes, and a 300 nm SiO_2 layer thermally grown onto silicon was used as the gate insulator. The SiO_2/Si substrates were washed in an ultrasonic bath using an Alconox solution (Alconox, Inc.), deionized water, isopropanol, and acetone for 10 min each; dried using N_2; and cleaned with oxygen plasma for 5 min (Harrick Plasma, 18 W). a-IGZO solutions were spin-coated onto substrates at 4000 rpm for 30 s, and the coated substrates were annealed at 320 °C for 30 min in air. The spin-coating step was repeated once. a-IGZO films were patterned by a conventional wet etching process using a negative photoresist (SU-8 2002, MicroChem). OSC IFL solutions were prepared under inert conditions. To obtain PCBM (Nano-C) and PCBM/N-DMBI (Sigma-Aldrich) solutions, 7 mg of PCBM was dissolved in 1 mL of chloroform, and 8.75 mg of N-DMBI was dissolved in 5 mL of chloroform, respectively. Each mixture was stirred at 50 °C for 1 h, and then the solutions were mixed to match the concentration (0, 1, 2 wt%) and stirred again at 50 °C for 30 min. To obtain a N2200 (Polyera) solution, 10 mg of N2200 was dissolved in 1 mL of chlorobenzene and stirred at 70 °C for 1 h. PCBM and N2200 solutions were spin-coated on the patterned a-IGZO film at 3000 rpm for 30 s and annealed at 50 and 120 °C, respectively. The thicknesses of PCBM IFL and N2200 IFL were 34 and 25 nm, respectively. Copper S/D electrodes (thickness = 50 nm) were deposited by thermal evaporation using an aluminum shadow mask with a channel width of 1500 µm and various channel lengths ranging from 25 to 350 µm. For selective N-DMBI doping, N-DMBI was deposited onto IFL films by thermal deposition using a shadow mask.

Device and Film Characterization: The current–voltage characteristics of the fabricated TFTs were measured in vacuum and ambient conditions using a Keithley 4200 SCS. The saturation mobilities (μ) and SS were calculated using the formulas

$$\mu_{sat} = (2I_{DS}L)/\left[WC_i(V_G - V_{th})^2\right] \quad \text{and} \quad SS = \left[d(V_G)\right]/\left[d(\log(I_{DS}))\right] \tag{1}$$

respectively, where I_{DS} is the S/D current, L is the channel length, W is the channel width, C_i is the areal capacitance of the gate dielectric, V_G is the gate voltage, and V_{th} is the threshold voltage. The surface morphology and film microstructure were characterized using an atomic force microscope (NX10, Park Systems) and GIXRD (D/MAX-2500, Rigaku). The GIXRD scan angle was varied between 3° and 70° using Cu Kα radiation (λ = 1.5418 Å) with a fixed incidence angle of 0.5°. TEM (JEM-ARM 200F, JEOL) was employed to investigate the structure of the multilayer TFTs at an acceleration voltage of 200 kV. The observed TEM samples were prepared by a focused ion beam (JIB-4601F, JEOL). The film thicknesses were determined using a profilometer (Dektak-XT, Bruker) for the IFL films and by TEM for the a-IGZO film. The electronic structures of the films were investigated by UV–visible spectroscopy (V-530, JASCO) and UV photoelectron spectroscopy (UPS, ESCALAB 250, Thermo Fisher Scientific). The photon energy of the UPS light source (He (I) radiation) was $h\nu$ = 21.2 eV, and the energy of the bandpass filter in the analyzer was fixed at 15 eV. Samples with a stack structure of a-IGZO (15 nm) on a conductive silicon substrate and PCBM (4–34 nm)/a-IGZO (15 nm) on a conductive silicon substrate were prepared. TOF SIMS (TOF SIMS 5, ION TOF) analysis in the depth-profile mode was performed to evaluate the migration of copper ions. Samples with a stack structure of Cu (50 nm)/a-IGZO (15 nm)/SiO_2 (300 nm) and Cu (50 nm)/PCBM (40 nm)/a-IGZO (15 nm)/SiO_2 (300 nm) on a conductive silicon substrate were prepared. A 1.5 mm wide metal layer was deposited on the top layers using the shadow-mask method. All samples were annealed at 150 °C for 1 h in air.

Supporting Information

Supporting Information is available from the Wiley Online Library or from the author.

Acknowledgements

This study was supported by Development of Space Core Program (2016M1A3A3A02016885), Basic Research Grant (2014R1A1A1036176), and Noncentrosymmetric Materials Bank (2014M3A9B8023478) through National Research Foundation of Korea grants funded by the Korean government (MSIP).

Received: December 31, 2016
Revised: February 7, 2017
Published online:

[1] a) T. Durkop, S. A. Getty, E. Cobas, M. S. Fuhrer, *Nano Lett.* **2004**, *4*, 35; b) R. L. Hoffman, B. J. Norris, J. F. Wager, *Appl. Phys. Lett.* **2003**, *82*, 733; c) Y. H. Kim, J. S. Heo, T. H. Kim, S. Park, M. H. Yoon, J. Kim, M. S. Oh, G. R. Yi, Y. Y. Noh, S. K. Park, *Nature* **2012**, *489*, 128; d) J. Liu, H. T. Zhang, H. L. Dong, L. Q. Meng, L. F. Jiang, L. Jiang, Y. Wang, J. S. Yu, Y. M. Sun, W. P. Hu, A. J. Heeger, *Nat. Commun.* **2015**, *6*, 10032; e) F. Schwierz, *Nat. Nanotechnol.* **2010**, *5*, 487; f) S. J. Seo, C. G. Choi, Y. H. Hwang, B. S. Bae, *J. Phys. D: Appl. Phys.* **2009**, *42*, 035106; g) Y. B. Yuan, G. Giri, A. L. Ayzner, A. P. Zoombelt, S. C. B. Mannsfeld, J. H. Chen, D. Nordlund, M. F. Toney, J. S. Huang, Z. N. Bao, *Nat. Commun.* **2014**, *5*, 3005; h) H. J. Yun, S. J. Kang, Y. Xu, S. O. Kim, Y. H. Kim, Y. Y. Noh, S. K. Kwon, *Adv. Mater.* **2014**, *26*, 7300.

[2] a) M. G. Kim, M. G. Kanatzidis, A. Facchetti, T. J. Marks, *Nat. Mater.* **2011**, *10*, 382; b) G. H. Kim, H. S. Kim, H. S. Shin, B. D. Ahn,

K. H. Kim, H. J. Kim, *Thin Solid Films* **2009**, *517*, 4007; c) B. H. Wang, X. G. Yu, P. J. Guo, W. Huang, L. Zeng, N. J. Zhou, L. F. Chi, M. J. Bedzyk, R. P. H. Chang, T. J. Marks, A. Facchetti, *Adv. Electron. Mater.* **2016**, *2*, 1500427; d) W. J. Lee, W. T. Park, S. Park, S. Sung, Y. Y. Noh, M. H. Yoon, *Adv. Mater.* **2015**, *27*, 5043; e) H. Y. Li, B. C. K. Tee, J. J. Cha, Y. Cui, J. W. Chung, S. Y. Lee, Z. N. Bao, *J. Am. Chem. Soc.* **2012**, *134*, 2760; f) Y. Diao, B. C. K. Tee, G. Giri, J. Xu, D. H. Kim, H. A. Becerril, R. M. Stoltenberg, T. H. Lee, G. Xue, S. C. B. Mannsfeld, Z. N. Bao, *Nat. Mater.* **2013**, *12*, 665.

[3] a) H. Yabuta, M. Sano, K. Abe, T. Aiba, T. Den, H. Kumomi, K. Nomura, T. Kamiya, H. Hosono, *Appl. Phys. Lett.* **2006**, *89*, 2123; b) N. Gong, C. Park, J. Lee, I. Jeong, H. Han, J. Hwang, J. Park, K. Park, H. Jeong, Y. Ha, Y. Hwang, *SID Int. Symp. Dig. Tech. Pap.* **2012**, *43*, 784.

[4] Y. H. Yang, S. S. Yang, C. Y. Kao, K. S. Chou, *IEEE Electron Device Lett.* **2010**, *31*, 329.

[5] a) J. K. Jeong, J. H. Jeong, J. H. Choi, J. S. Im, S. H. Kim, H. W. Yang, K. N. Kang, K. S. Kim, T. K. Ahn, H.-J. Chung, M. Kim, B. S. Gu, J.-S. Park, Y.-G. Mo, H. D. Kim, H. K. Chung, *SID Int. Symp. Dig. Tech. Pap.* **2008**, *39*, 1; b) S. Jeon, S. Park, I. Song, J. H. Hur, J. Park, H. Kim, S. Kim, S. Kim, H. Yin, U. I. Chung, E. Lee, C. Kim, *ACS Appl. Mater. Interfaces* **2011**, *3*, 1; c) H. T. Chen, Y. Cao, J. L. Zhang, C. W. Zhou, *Nat. Commun.* **2014**, *5*, 4097; d) T. Arai, *J. Soc. Inf. Disp.* **2012**, *20*, 156.

[6] a) J. Jeong, G. J. Lee, J. Kim, B. Choi, *Appl. Phys. Lett.* **2012**, *100*, 112109; b) Y. H. Tai, H. L. Chiu, L. S. Chou, *J. Electrochem. Soc.* **2012**, *159*, J200.

[7] a) P. S. Yun, J. Koike, *J. Electrochem. Soc.* **2011**, *158*, H1034; b) Z. H. Cao, K. Hu, X. K. Meng, *J. Appl. Phys.* **2009**, *106*, 113513; c) S. H. Lee, D. J. Oh, A. Y. Hwang, D. S. Han, S. Kim, J. K. Jeong, J. W. Park, *IEEE Electron Device Lett.* **2015**, *36*, 802; d) A. Hino, T. Maeda, S. Morita, T. Kugimiya, *J. Inf. Disp.* **2012**, *13*, 61.

[8] H. W. Zan, W. W. Tsai, C. H. Chen, C. C. Tsai, *Adv. Mater.* **2011**, *23*, 4237.

[9] R. A. Street, T. N. Ng, R. A. Lujan, *ACS Appl. Mater. Interfaces* **2014**, *6*, 4428.

[10] a) D. H. Kang, I. Kang, S. H. Ryu, Y. S. Ahn, J. Jang, *J. Disp. Technol.* **2013**, *9*, 699; b) M. D. H. Chowdhury, M. Mativenga, J. G. Um, R. K. Mruthyunjaya, G. N. Heiler, T. J. Tredwell, J. Jang, *IEEE Trans. Electron Devices* **2015**, *62*, 869; c) S. Y. Huang, T. C. Chang, M. C. Chen, S. C. Chen, C. T. Tsai, M. C. Hung, C. H. Tu, C. H. Chen, J. J. Chang, W. L. Liau, *Electrochem. Solid-State Lett.* **2011**, *14*, H177.

[11] a) J. H. Na, M. Kitamura, Y. Arakawa, *Appl. Phys. Lett.* **2008**, *93*, 063501; b) J. R. Yim, S. Y. Jung, H. W. Yeon, J. Y. Kwon, Y. J. Lee, J. H. Lee, Y. C. Joo, *Jpn. J. Appl. Phys.* **2012**, *51*, 011401; c) S. K. Park, Y. H. Kim, J. I. Han, *J. Phys. D: Appl. Phys.* **2009**, *42*, 125102; d) Y. Shimura, K. Nomura, H. Yanagi, T. Kamiya, M. Hirano, H. Hosono, *Thin Solid Films* **2008**, *516*, 5899.

[12] a) A. Suresh, J. F. Muth, *Appl. Phys. Lett.* **2008**, *92*, 033502; b) J. W. Hennek, Y. Xia, K. Everaerts, M. C. Hersam, A. Facchetti, T. J. Marks, *ACS Appl. Mater. Interfaces* **2012**, *4*, 1614; c) P. Barquinha, A. M. Vila, G. Goncalves, R. Martins, J. R. Morante, E. Fortunato, L. Pereira, *IEEE Trans. Electron Devices* **2008**, *55*, 954.

[13] a) D. Q. Zhang, R. R. Wang, M. C. Wen, D. Weng, X. Cui, J. Sun, H. X. Li, Y. F. Lu, *J. Am. Chem. Soc.* **2012**, *134*, 14283; b) C. Hwang, J. An, B. D. Choi, K. Kim, S. W. Jung, K. J. Baeg, M. G. Kim, K. M. Ok, J. Hong, *J. Mater. Chem. C* **2016**, *4*, 1441.

[14] C. K. Lee, S. Y. Park, H. Y. Jung, C. K. Lee, B. G. Son, H. J. Kim, Y. J. Lee, Y. C. Joo, J. K. Jeong, *Phys. Status Solidi RRL* **2013**, *7*, 196.

[15] a) T. L. Ho, *Chem. Rev.* **1975**, *75*, 1; b) L. H. Lee, in *Surfactants and Macromolecules: Self-Assembly at Interfaces and in Bulk* (Eds: B. Lindman, J. B. Rosenholm, P. Stenius), Steinkopff, Darmstadt, Germany **1990**, p. 337; c) A. Alfarra, E. Frackowiak, F. Beguin, *Appl. Surf. Sci.* **2004**, *228*, 84.

[16] a) W. Sliwa, M. Deska, *ARKIVOC* **2008**, *87*, 127; b) W. L. Chou, K. C. Yang, *J. Hazard. Mater.* **2008**, *154*, 498.

[17] K. Ide, Y. Kikuchi, K. Nomura, M. Kimura, T. Kamiya, H. Hosono, *Appl. Phys. Lett.* **2011**, *99*, 093507.

[18] J. K. Jeong, H. W. Yang, J. H. Jeong, Y. G. Mo, H. D. Kim, *Appl. Phys. Lett.* **2008**, *93*, 123508.

[19] N. J. Zhou, M. G. Kim, S. Loser, J. Smith, H. Yoshida, X. G. Guo, C. Song, H. Jin, Z. H. Chen, S. M. Yoon, A. J. Freeman, R. P. H. Chang, A. Facchetti, T. J. Marks, *Proc. Natl. Acad. Sci. USA* **2015**, *112*, 7897.

[20] S. P. Schiessl, H. Faber, Y. H. Lin, S. Rossbauer, Q. X. Wang, K. Zhao, A. Amassian, J. Zaumseil, T. D. Anthopoulos, *Adv. Mater.* **2016**, *28*, 3952.

[21] a) C. R. Kagan, D. B. Mitzi, C. D. Dimitrakopoulos, *Science* **1999**, *286*, 945; b) H. B. Wang, Z. T. Liu, M. F. Lo, T. W. Ng, C. S. Lee, D. H. Yan, S. T. Lee, *J. Appl. Phys.* **2010**, *107*, 024510.

[22] a) G. Huang, L. Duan, G. Dong, D. Zhang, Y. Qui, *ACS Appl. Mater. Interfaces* **2014**, *6*, 20786; b) Y. S. Rim, H. Chen, X. Kou, H. S. Duan, H. Zhou, M. Cai, H. J. Kim, Y. Yang, *Adv. Mater.* **2014**, *26*, 4273; c) S. Y. Lee, S. Chang, J. S. Lee, *Thin Solid Films* **2010**, *518*, 3030.

[23] Y. H. Han, J.-Y. Won, H.-S. Yoo, J.-H. Kim, R. Choi, J. K. Jeong, *ACS Appl. Mater. Interfaces* **2016**, *8*, 1156.

[24] C. Amit, *J. Semicond.* **2013**, *34*, 066001.

[25] a) C. Liu, Y. Xu, Y. Y. Noh, *Mater. Today* **2015**, *18*, 79; b) W. Wang, L. Li, C. Lu, Y. Liu, H. Lv, G. Xu, Z. Ji, M. Liu, *Appl. Phys. Lett.* **2015**, *107*, 063504.

[26] a) P. Wei, J. H. Oh, G. F. Dong, Z. N. Bao, *J. Am. Chem. Soc.* **2010**, *132*, 8852; b) B. D. Naab, S. Guo, S. Olthof, E. G. B. Evans, P. Wei, G. L. Millhauser, A. Kahn, S. Barlow, S. R. Marder, Z. N. Bao, *J. Am. Chem. Soc.* **2013**, *135*, 15018; c) S. Rossbauer, C. Müller, T. Anthopoulos, *Adv. Funct. Mater.* **2014**, *24*, 7116; d) J. H. Ok, P. Wei, Z. N. Bao, *Appl. Phys. Lett.* **2010**, *97*, 243305; e) P. Wei, T. Menke, B. D. Naab, K. Leo, M. Riede, Z. N. Bao, *J. Am. Chem. Soc.* **2012**, *134*, 3999; f) H. Wang, P. Wei, Y. Li, J. Han, H. R. Lee, B. D. Naab, N. Liu, C. Wang, E. Adijanto, B. C. -K. Tee, S. Morishita, Q. Li, Y. Gao, Y. Cui, Z. N. Bao, *Proc. Natl. Acad. Sci. USA* **2014**, *111*, 4776.

[27] W. T. Chen, S. Y. Lo, S. C. Kao, H. W. Zan, C. C. Tsai, J. H. Lin, C. H. Fang, C. C. Lee, *IEEE Electron Device Lett.* **2011**, *32*, 1552.

[28] W. G. Kim, Y. J. Tak, B. D. Ahn, T. S. Jung, K. B. Chung, H. J. Kim, *Sci. Rep.* **2016**, *6*, 23039.

[29] K. Nomura, T. Kamiya, H. Hosono, *Appl. Phys. Lett.* **2011**, *99*, 053505.